

Highly efficient and bifunctional Cd(II)-Organic Framework platform towards Pb(II), Cr(VI) detection and Cr(VI) photoreduction



Ling-Hui Chen¹, Xin-Bin Cai¹, Qing Li^{*}, Bin-Bin Guan, Tian-Hui Liu, Dan Li, Zhi-Qiang Wu, Wei Zhu^{**}

Xi'an Key Laboratory of Textile Chemical Engineering Auxiliaries, School of Environmental & Chemical Engineering, Xi'an Polytechnic University, Xi'an, 710048, PR China

ARTICLE INFO

Keywords:

Cadmium-organic framework
Fluorescent detection and reduction
Pb(II) and Cr(VI)
Recyclable
Sensing and reducing mechanism

ABSTRACT

Lead and chromate/dichromate are widely used in manufacturing industry, but Pb(II) and Cr(VI) ions pose fatal threats to human health and the water ecological environment. It is thus highly desirable to develop novel and valid strategies for rapid detection and effective decontamination of these heavy metal ions. Design and assembly of luminescent Metal-Organic Framework (LMOFs) for effective recognition and removal of Pb(II) and/or Cr(VI) from water provide a feasible avenue to address this issue. Herein, a novel Cd(II)-MOF, [(Cd₃L₂)]_x(solvent)_x (labeled as compound **1**) with bright blue fluorescence was assembled under the solvothermal reaction of triangular ligand 5'-(5-carboxy-1H-benzo [d]imidazole-2-yl)-[1,1':3',1''-terphenyl]-4,4''-dicarboxylic acid (H₃L) and Cd(NO₃)₂. Given that the unique structure features of 3D stacking framework, i. e. strong π···π conjugative effects of organic linkers, plentiful free imidazole N atoms and carboxyl O atoms, Cd-MOF of **1** was deliberately deployed as bifunctional platform to sense Pb(II)/Cr(VI) and photochemically reduce Cr(VI) to Cr(III). Notably, **1** emits durable bright blue fluorescence and performs rapid quenching sense for Pb²⁺, Cr₂O₇²⁻ and CrO₄²⁻, with ultra low detection limits of 1.89, 4.83 and 2.84 ppb, respectively. Moreover, highly toxic Cr(VI) could be rapidly and thoroughly reduced to Cr(III) ions by **1** under the irradiation of mercury lamp, with reliable recycling ability. The possible photoluminescence, quenching and photocatalytic reduction mechanisms also were tentatively proposed.

1. Introduction

Heavy metal ions, such as positive divalent Pb(II) of Pb²⁺ and hexavalent Cr(VI) of Cr₂O₇²⁻/CrO₄²⁻ have been used for centuries by human beings, still play irreplaceable roles in many fields such as chemical industry, metallurgy, leather and pigments [1–5] et al. However, both of them are deadly toxic contaminants for underground and surface water systems, which will cause a series of fatal hazards like carcinogenesis and mutagenicity even at the trace grade of concentration [6,7]. The maximum contaminant limits of Pb(II) and Cr(VI) ions in drinking water have been set to be 0.05 and 0.01 mg L⁻¹ by some authorities, respectively. The two highly toxic heavy metal ions thus should be effectively monitored and efficiently removed from water at any cost. Although precision instrument analysis and chemical titration methods have been widely adopted to identify/detect Pb(II) and Cr(VI) ions, high cost and time-consuming are extremely detrimental for practical applications

[8–12]. In addition, various methods including but not limited to chemical precipitation, physical capture, membrane separation etc have been widely deployed to decontaminate Pb(II) and Cr(VI) ions [13–18]. Prominently, the most preferred remediation towards wastewater contained Cr(VI) is to convert highly toxic Cr(VI) to lowly toxic Cr(III), which is easily converted to Cr(OH)₃ precipitation and completely removed. Compared with electroreduction and chemical reduction methods, photocatalytic reduction of Cr(VI) to Cr(III) by highly active photocatalyst is more effective and economical, and will not produce other secondary pollutants [19–21]. Therefore, it is highly imperative to develop a novel bifunctional material for effective Pb(II), Cr(VI) detection and Cr(VI) photoreduction.

Metal-Organic Frameworks (MOFs), as a new type of solid-state crystalline organic-inorganic hybrid materials, have developed into a versatile functional platform with not only intriguing aesthetic structures but also excellent properties e. g. fluorescence detection, physical

^{*} Corresponding author.

^{**} Corresponding author.

E-mail addresses: liqingxpu1@163.com (Q. Li), zhuwei@xpu.edu.cn (W. Zhu).

¹ These authors contributed equally to this work.

capture, photochemical decontamination of toxic pollutants [22–27] and some applications in energy related fields [28–31]. Compared with non-porous optical probe, luminescence MOFs (LMOFs) combine permanent porosity, tunable structures and optical performances. Owing to their advantages of low cost, low detection limit (DL), high sensitivity and selectivity et al., LMOFs have been considered to be one of the most promising photochemical probes for sensing Pb(II) and Cr(VI) ions [32–35]. Particularly, LMOFs modified with abundant free active groups (anchoring sites) such as unsaturated coordinated carboxyl O atoms, pyridine or imidazole N atoms, are apt to coordinate with free target analytes, leading to fluorescent quenching or other responses in MOFs' luminescence [36–39]. Moreover, considering the inorganic-organic hybrid features of MOFs, central metal ions will coordinate with, for example, carboxyl oxygen atoms to form plentiful M – O nodes, which perform typical characteristics of inorganic semiconductors [27,40]. As optical absorption antenna, the coordinated aromatic organic linkers with excellent photosensitivity can effectively capture light energy, and then transfer the photogenerated electrons from conduction bands (CB) to Cr(VI) centre for reduction [41]. Compared with traditional catalysts, MOFs based catalysts have attracted much attention due to their high photocatalytic efficiency, high recycling ability and less secondary pollution [20,42]. However, considering the poor selectivity, sensitivity, low photocatalytic reduction efficiency and reaction kinetics, and/or the single functionality in a single MOFs platform, it is therefore highly imperative to open an ideal avenue for realizing highly effective detection and efficient removal of Pb(II)/Cr(VI) ions from water, by designing novel MOFs materials with bifunctional fluorescence sensing response and photocatalytic reduction activity.

Based on the above hypothesis and consideration, a new Cd-MOF, $[(Cd_3L_2)] \cdot (\text{solvent})_x$ (labeled as compound 1, $H_3L = 5'$ -(5-carboxy-1H-benzo [d]imidazole-2-yl)-[1,1':3',1''-terphenyl]-4,4''-dicarboxylic acid) was deliberately designed by us. The assemble of tetrahedral

$[Cd(O_2C-)_3N]$ nodes and asymmetric triangular linkers H_3L provides a 2D framework cross-linked with two closely adjacent/parallel single networks, and further presents a 3D stacking framework with stretched hexagonal channels decorated by plenty of free imidazole N atoms and unsaturated coordinated carboxyl O atoms. For Cd-MOF of 1, the immobilization of highly conjugated organic ligands, sharp proximity from each other and the dense stacking of the 2D network tend to generate strong $\pi \cdots \pi$ conjugative effects, which are beneficial for its photosensitivity and luminescence abilities [43]. While the presence of abundant active groups provides anchoring sites towards free Pb(II) and Cr(VI) ions in aqueous solution, and then leads to highly sensitive fluorescence sensing of 1 [44]. It is worth noting that compound 1 presents immediate and effective fluorescence quenching sensing toward Pb(II), Cr(VI) ions, with ultra-low detection limits (DL), rather high quenching constant (K_{sv}) value. Particularly the efficient and rapid photochemical removal ability in reducing Cr(VI) to Cr(III) ions with reliable photocatalytic cycle talent. The dual-functionality of 1 in efficiently probing Pb(II), Cr(VI) and purifying Cr(VI) from water was confirmed and the related mechanisms also was studied in detail.

2. Results and discussion

2.1. Description of the crystal structure of 1

Block-shaped and colorless 1 was synthesized by tritopic H_3L linkers and Cd(II) nodes under solvothermal reaction in an N,N'-dimethylformamide (DMF)/water solution (Fig. 1a), formulated as $[(Cd_3L_2)] \cdot (\text{solvent})_x$ (1) from Single-crystal X-ray diffraction (SCXRD) detail. Phase purity of crystal samples was confirmed by flawlessly matched powder X-ray diffraction (PXRD) patterns between the simulated and stacks of as-synthesized crystals (Fig. S1). According to SCXRD data, Cd-MOF of 1 crystallizes in monoclinic system, $I2/c$ space group

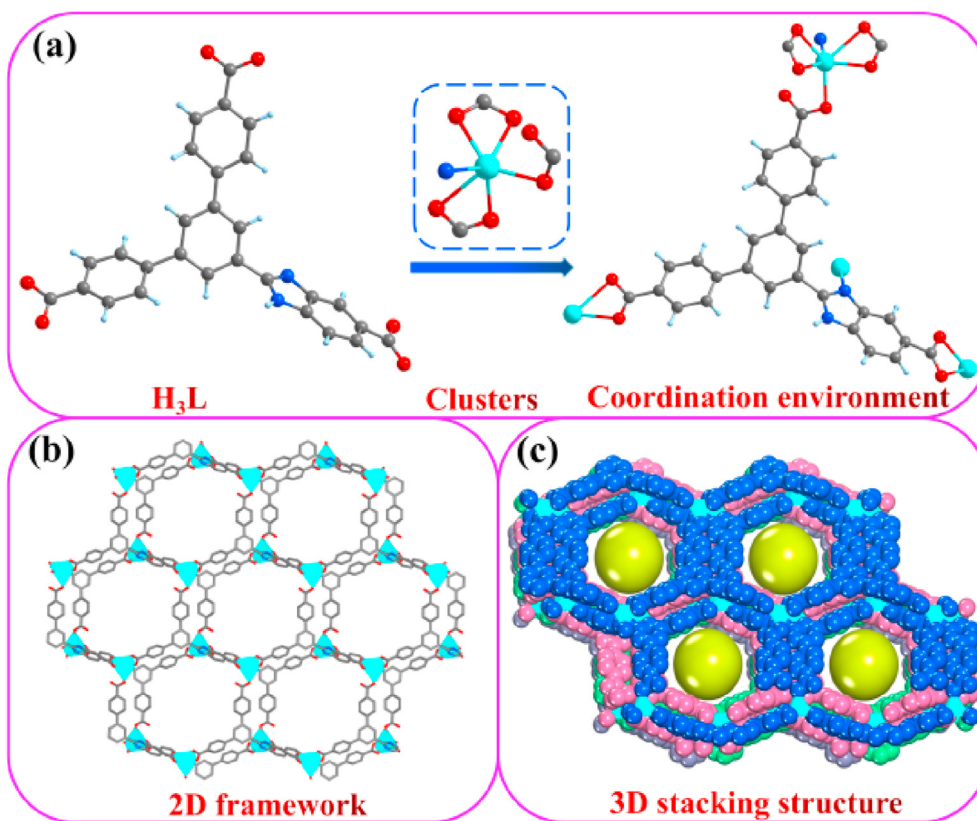


Fig. 1. Schematic representation for assembling Cd-MOF of 1: (a) Construction of repeated structural units of 1 with uncoordinated carboxyl oxygen atoms and imidazole nitrogen atoms. (b) 2D framework and (c) the final 3D stacking structure with hexagonal channels along a -axis.

(Table S1 in section S11). In the asymmetric unit of **1**, there exist one kind of crystallographically independent Cd^{2+} ion furnished by five-surrounding carboxylate O atoms and non-hydroimidazole N atoms, respectively (Fig. 1a). Similar tetrahedral $[\text{Cd}(\text{O}_2\text{C}-)_3(\text{N})]$ SBUs are assembled and accomplished by mono-dentate carboxylate, chelating carboxylates and mono-dentate imidazole nitrogen atom for Cd(II) centre. The unique SBUs are interconnected by the conjugated tritopic L linkers to present a 2D plane formed with two parallel single nets which are firmly locked by neighboring imidazole N atoms and Cd(II) nodes (Fig. 1b). Then, the 2D planes are further stacked to form a final 3D framework with regularly stretched hexagonal channels along *a*-axis ($8.64 \times 10.2 \text{ \AA}^2$, considering van der Waals radii), which are decorated with free O, N atoms from unsaturated coordinated carboxyl and benzimidazole groups (Fig. 1c). Compared with reported Cd-MOFs, **1** comprises uncoordinated N and O atoms, which may provide more possibilities for **1** to interact with the target Pb(II) and Cr(VI) ions to realize more sensitive fluorescence probing. In addition, strong $\pi \cdots \pi$ stacking generated within one single 2D plane (3.453–3.529 \AA) and between the two neighboring but independent nets (3.579–4.031 \AA) of **1** not only can increase its stability but also may strengthen the application performances. Furthermore, thermal weightloss curve and fourier transform infrared spectra of **1** also were tested and analyzed (Figs. S2 and S3).

2.2. Photoluminescence properties

2.2.1. Photoluminescence of **1** and H_3L in water

After being uniformly ground and ultrasonically dispersed into deionized water, the photoluminescence performances of Cd-MOF of **1** and ligand H_3L were recorded over fluorescence spectrophotometer. Indeed, **1** emits bright blue fluorescence with a maximum emission wavelength of 373 nm, under the excitation of exciting light at 279 nm (Fig. 2). Interestingly, as revealed in Fig. S4, compared with the apparently weak emission peak intensity at 376 nm for free H_3L and ineffective emission performance of fresh $\text{Cd}(\text{NO}_3)_2$, rigid framework of **1** presents an obviously strengthened fluorescence emission capability with a blue-shifted of 3 nm. Interestingly, under the same concentration of 16 mg L^{-1} , a brighter luminescence of **1** than H_3L could be observed under the irradiation of ultraviolet light at 254 nm (inserted photos in Fig. 2).

2.2.2. Water stability and appropriate concentration of **1**

Considering that water stability is an important parameter for a practical photochemical probe, changes of maximum fluorescence

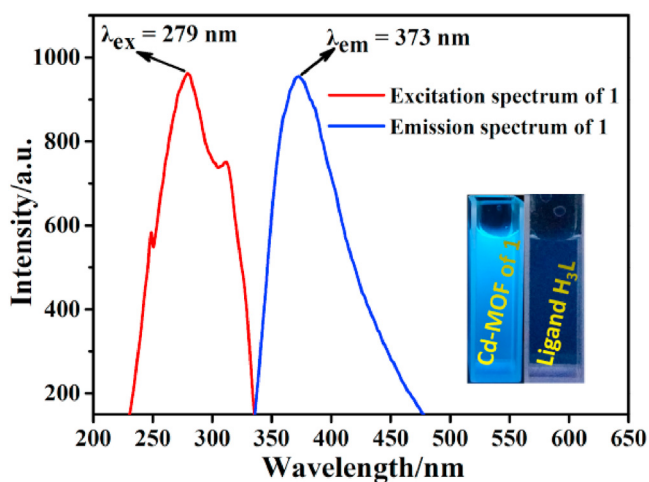


Fig. 2. Luminescence excitation (red) and emission (blue) spectrum for **1**; aqueous suspensions of **1** and H_3L under irradiation of ultraviolet light at 254 nm (inserted photos). (For interpretation of the references to color in this figure legend, the reader is referred to the Web version of this article.)

emission intensity for the aqueous suspension of **1** was studied in detail in consecutive 14 days at room temperature. As shown in Figs. S1 and S5a, it is worth noting that the excellently maintained photoluminescence properties of **1** matched well with its flawlessly preserved PXRD patterns underwent being immersed in aqueous solution for 3, 5 and 14 days. Moreover, the unattenuated luminescence intensity visible to the naked eyes also provided a good evidence to confirm the persistence of the luminescence intensity from **1** (Fig. S5b). Furthermore, 16 mg L^{-1} was confirmed to be the most suitable concentration for the aqueous suspension of **1** to release the maximum emission intensity (Fig. S6).

2.3. Fluorescent quenching sensing towards cationic Pb(II)

Given that the neutral framework of **1** rich in free active sites (carboxyl oxygen and benzimidazole N atoms), which provides the possibility for guest analytes such as heavy metal ions to interact with the Cd-MOF skeleton, and then change its original luminescence performances to achieve recognition and detection functionality [45]. Here, Pb^{2+} ions were deployed as target analyte to be detected by **1** in deionized water. Clearly, as demonstrated in Fig. S7, as gradually increased the concentration of Pb^{2+} ions from 0.3 to 30.0 μM , the bright blue fluorescence from aqueous suspension of **1** under the irradiation of UV-light at 254 nm attenuated quickly and eventually quenched completely, proving that Cd-MOF of **1** can act as a fluorescent quenching probe to detect Pb(II) ions. In addition, as exhibited in Fig. S8, the instantaneous and durable responsiveness of **1** in sensing Pb(II) ions also has been confirmed. Because after 50 μL Pb(II) ions ($4.5 \times 10^{-4} \text{ M}$) were added into 3 mL aqueous suspension of **1** and mixed well quickly, its fluorescence emission intensity immediately decreased from 946.51 to 786.23. Prominently, the perfectly maintained fluorescence emission intensity of **1** was experimentally confirmed by monitoring once every 0.06 s within the next 500 s.

2.3.1. Selective and anti-interference properties of **1** in sensing Pb(II)

For heavy metal ions i. e. Pb^{2+} , it often coexist with other metal cations and anions in environmental water bodies, thus the selective detection and effective identification of target analytes by excluding the interference of external complicated ions are crucial for a qualified fluorescent probe [46]. In order to further assess the actual detection capability of **1** for Pb^{2+} , selective detection experiments were firstly performed by simulating some cationic analytes from nitrate salts of $\text{X}_1(\text{NO}_3)_n$ ($\text{X}_1 = \text{Na}^+, \text{Cd}^{2+}, \text{Cr}^{3+}, \text{Mg}^{2+}, \text{K}^+, \text{Cu}^{2+}, \text{Fe}^{3+}, \text{Ag}^+, \text{Co}^{2+}$ or Ni^{2+}) and anionic species from potassium salts of K_nX_2 ($\text{X}_2 = \text{I}^-, \text{F}^-, \text{IO}_3^-, \text{NO}_2^-, \text{Cl}^-, \text{Br}^-, \text{SO}_4^{2-}, \text{SCN}^-, \text{C}_2\text{H}_5\text{O}^-, \text{PO}_4^{3-}, \text{CO}_3^{2-}$ or HPO_4^{2-}). Herein, 50 μL above prepared $\text{X}_1(\text{NO}_3)_n$ or K_nX_2 all of which with the concentration of $1.8 \times 10^3 \mu\text{M}$ was added into a quartz cuvette containing 3 mL aqueous suspension of **1** to obtain a series of 30 μM two-component aqueous suspensions labeled as 1- X_1 and 1- X_2 , respectively. Evidently, as soon as Pb^{2+} invaded the aqueous suspension of **1** in quartz cuvette, almost complete fluorescent quenching occurred (Fig. 3a and b) instantaneously. However, for other 1- X_1 and 1- X_2 systems, only relatively slight or negligible fluorescence emission intensity changes could be observed, indicating that **1** can identify and detect Pb^{2+} with high selectivity from water, compared with many other cations and anions.

Moreover, the single or mixed cations/anions may coexist with the target analytes in actual water environment, whether the highly selective detection ability of **1** still can be well preserved in the presence of other interfering ions should be studied in detail [47]. As shown in Fig. 4, the competitive detection experiments results confirmed that Cd-MOF of **1** can available suppress the influence of single cationic/anionic interference in probing Pb^{2+} ions. That is, for various competitive combinations such as $(\text{Pb}^{2+} + \text{X}_1)$ or $(\text{Pb}^{2+} + \text{X}_2)$, the fluorescence quenching efficiencies $[(I_0 - I)/I_0]\%$ of **1** caused by guest Pb^{2+} are still as high as over 92%. More interestingly, compared with blank sample, after 50 μL mixture of all the above single ions with the total concentration of $1.8 \times 10^3 \mu\text{M}$ (Fig. S9) was added into 3 mL fresh aqueous suspension of **1** to obtain a new

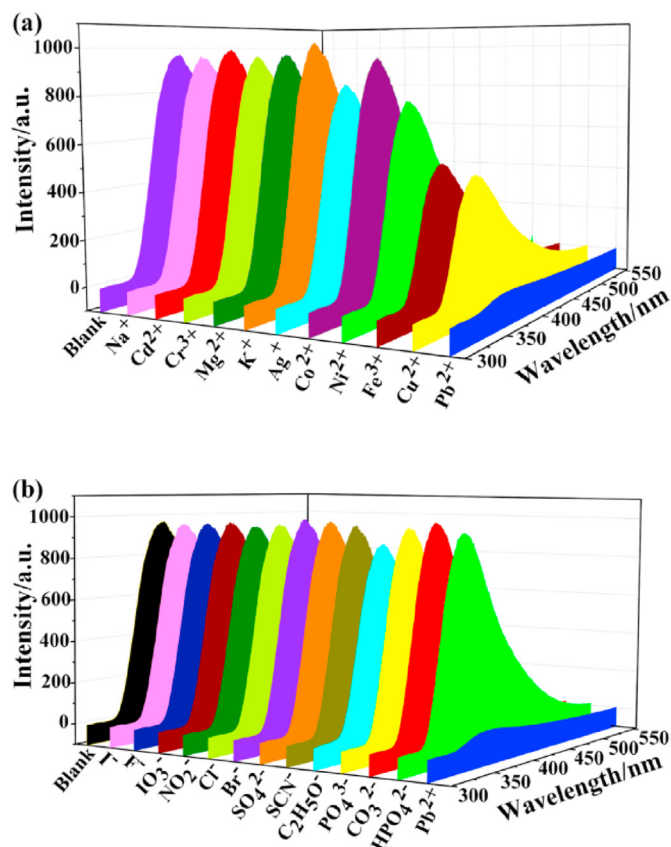


Fig. 3. Relative fluorescence intensities at 373 nm for the aqueous suspension of 1 after adding different cationic (a) or anionic (b) analyte.

suspension of 1-X' (X' = all the mixture of X₁ and X₂), the fluorescence emission intensity were still maintained to be 92.27%. Nevertheless, as soon as 50 μ L Pb²⁺ ion of 1.8×10^3 μ M invaded the system of 1-X', immediate fluorescence quenching response was recorded with a fairly high quenching efficiency of 98.21%. Combined with the above results, Cd-MOF of 1 can undoubtedly play the role of photochemical sensor in probing Pb(II) ions with excellent selectivity and anti-interference ability.

2.3.2. Sensitivity and detection limit (DL) towards Pb(II) ions

Detection sensitivity, which is usually quantified as detection limit (DL), is an important indicator for practical fluorescent probe. Herein, detail fluorescence titration experiments were performed by gradually adding different concentrations of Pb²⁺ ions into the aqueous suspension of 1. As clearly illustrated in Fig. 5a, as the concentration of Pb²⁺ ions increased from 0 to 30 μ M, the fluorescence emission intensity curves of 1 at 373 nm slowly decreased from original 946.51 to eventually become almost a smooth line. And the change process of fluorescence emission curves also match well with the fluorescence quenching details visible to the naked eyes (Fig. S7). In addition, the fluorescence quenching constant, often known as the K_{sv} value, was calculated by Stern-Volmer equation $I_0/I = 1 + K_{sv}[M]$ to quantitatively evaluate the detection sensitivity of 1, where I_0 and I are the fluorescence emission intensity of 1 in aqueous suspension before and after invaded by Pb²⁺, $[M]$ represents the molar concentration of analyte ions. Prominently, the results exhibited in Fig. 5b reveal that as gradually increased the concentrations of Pb²⁺ ions, a good linear relationship between I_0/I and concentrations could be obtained. And the K_{sv} value was calculated to be 2.4×10^4 M⁻¹, rather high a value for all reported MOF-based fluorescent sensing probes. The DL value was calculated by $3S_b/S$, where S_b and S represent the standard deviation of blank measurement and the slope of the

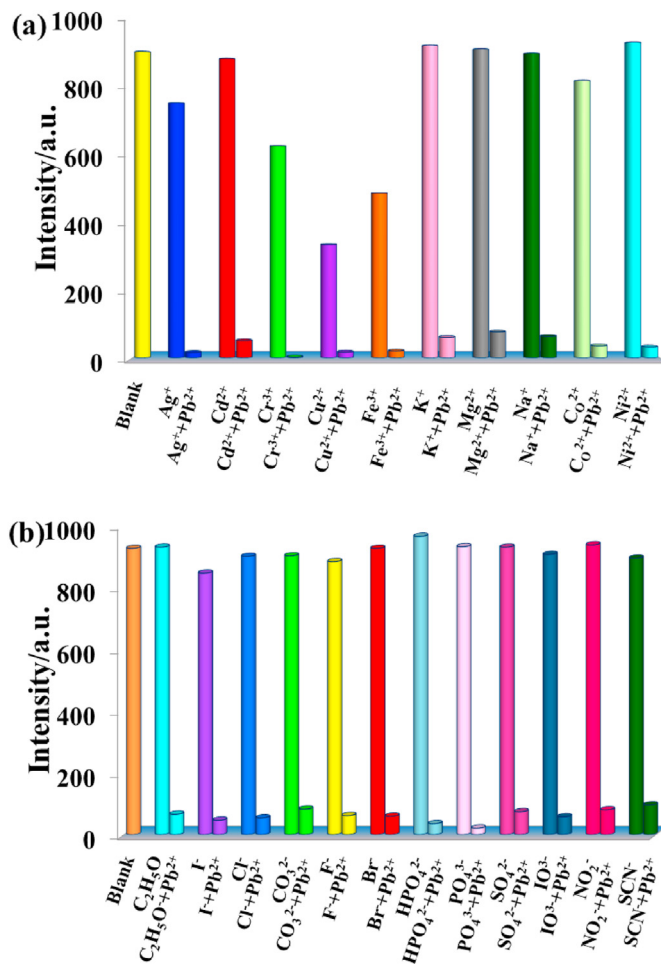


Fig. 4. The fluorescence changes of 1 (16 mg L^{-1}) upon the addition of various anions and metal cations ($1.8 \times 10^3 \text{ M}$) and Pb(NO₃)₂ ($1.8 \times 10^3 \text{ M}$) in aqueous solution. Left-hand bars represent the fluorescent responses toward anions; Right-hand bars represent the subsequent addition of Pb(NO₃)₂ to the aforementioned solutions.

calibration curve, respectively. Here, according to the calculation formula as shown in supporting information (Section S3) [48], the DL value of 1 in sensing Pb²⁺ ions was confirmed to be 1.89 ppb, which is one of the smallest values among all MOFs so far (Table S2).

2.4. Fluorescence quenching sensing towards anionic Cr(VI)

Considering the neutral framework properties of compound 1, Cd-MOF may theoretically interact with both cations and anions. So, another representative highly toxic anion i. e. Cr(VI) in the form of Cr₂O₇²⁻ and CrO₄²⁻, was selected as the target analyte for recognition and detection using Cd-MOF of 1 as fluorescent sensing probe.

As clearly exhibited in Fig. S10, the bright blue luminescence (fluorescence emission intensity) of compound 1 gradually darkened until the luminescence disappeared completely, as the concentrations of Cr₂O₇²⁻ and CrO₄²⁻ in the aqueous suspension solution of 1 increasing from 0 to 390 and 0–675 μ M, respectively. Furthermore, the instantaneous and durable fluorescence quenching responsiveness of 1 in probing both Cr₂O₇²⁻ and CrO₄²⁻ ions also were systematically researched. As demonstrated in Figs. S11a and 11b, the fluorescence emission intensities of Cr₂O₇²⁻ and CrO₄²⁻ decreased immediately from original 945.29 to final 514.26, as soon as 50 μ L Cr(VI) ions ($2.7 \times 10^{-3} \text{ M}$) were introduced and well distributed into the aqueous suspension of 1 (3 mL). More interestingly, the fluorescence emission intensities of 514.26 for 1 also were flawlessly preserved, according to the recorded results on fluorescence

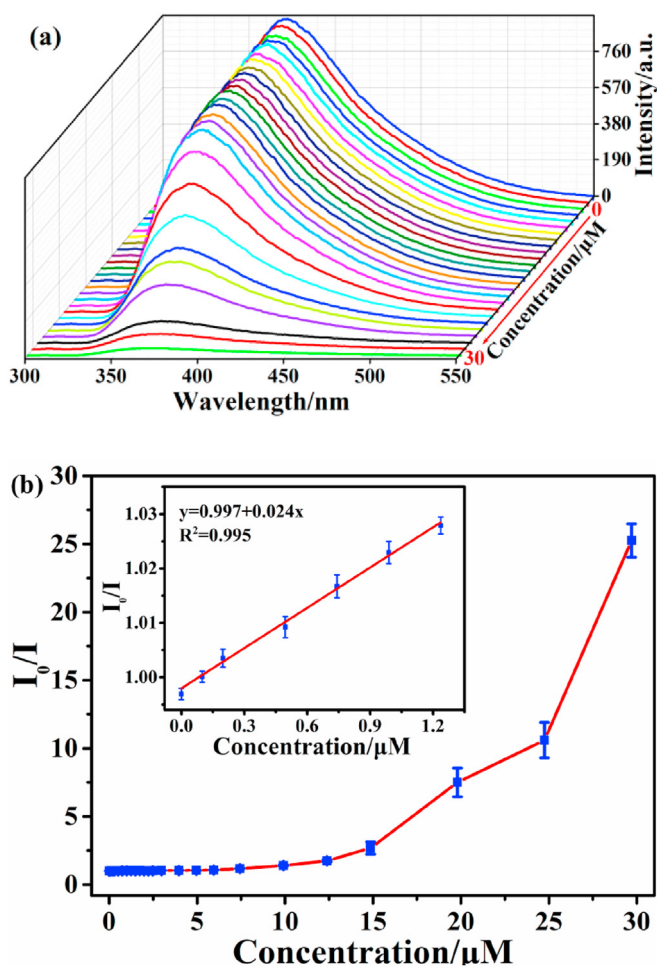


Fig. 5. Fluorescence responses of **1** towards Pb(II) in aqueous solution: (a) Concentration-dependent luminescence quenching of **1** after adding Pb²⁺ with different concentrations. (b) Stern-Volmer plot of I_0/I versus the concentrations of Pb(II) in the aqueous suspension of **1**.

spectrophotometer once every 0.06 s within the next 500 s.

2.4.1. Selective and anti-interference properties for sensing Cr(VI) anions

For anionic Cr(VI) analytes, they also usually co-exist with other anions in real water environment. The interference of external anions thus can not be ignored for sensing both Cr₂O₇²⁻ and CrO₄²⁻ ions by Cd-MOF of **1**. Here, potassium salts of K_nX₂ were adopted as control analytes and the experimental parameters are exactly the same as the ones deployed in section 2.3.1. Notably, just as verified in previous experiments, the invasion of common anions i. e. I⁻, F⁻, IO₃⁻, NO₂⁻, Cl⁻, Br⁻, SO₄²⁻, SCN⁻, C₂H₅O⁻, PO₄³⁻, CO₃²⁻ or HPO₄²⁻ has little effect on the fluorescence emission intensity of compound **1** (Fig. 6). But the almost complete quenching response occurred instantly, as soon as the framework of **1** was exposed to either Cr₂O₇²⁻ or CrO₄²⁻ ion, performing fairly high quenching efficiencies of 98.77% and 99.89%, respectively. Moreover, as exhibited in Fig. S12, Cd-MOF of **1** still can easily identify and detect the target analytes in (Cr₂O₇²⁻ + X₂) and (CrO₄²⁻ + X₂) two-component combinations. More prominently, as revealed in Figs. S13a and S13b, compared with the blank sample, after 50 μL mixture of all the above single anions with the total concentration of 2.7 × 10⁻² M was added into 3 mL fresh aqueous suspension of **1** to obtain new suspension of 1-X₂' (X₂' = the mixture of all single X₂), the fluorescence emission intensity were still maintained to be 98.04% and 99.47%. Nevertheless, after 50 μL Cr₂O₇²⁻ or CrO₄²⁻ ions of 2.7 × 10⁻² M was introduced into the system of 1-X₂', immediate fluorescence quenching response was monitored with rather high quenching efficiencies of 99.34% and 99.82%.

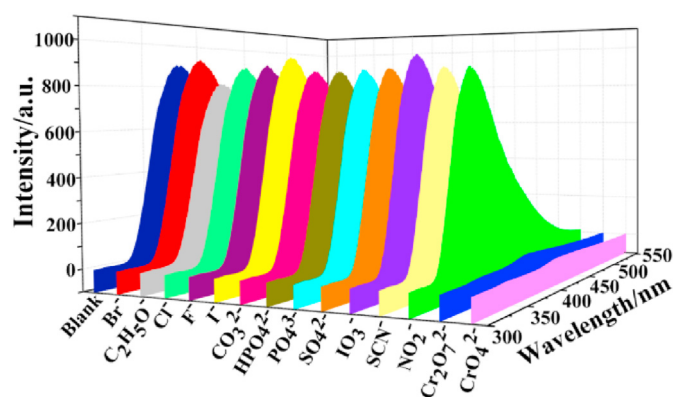


Fig. 6. Relative fluorescence intensities at 373 nm for the aqueous suspension of **1** after adding different anionic analytes. (The concentration of all anions was 2.7 × 10⁻² M).

Based on the above findings, Cd-MOF of **1** can undoubtedly play an outstanding role of photochemical sensor in sensing both Cr(VI) and Pb(II) ions with reliable selectivity and anti-interference ability.

2.4.2. Sensitivity and detection limit (DL) towards Cr(VI)

To further assess the sensitivity and DL value of **1** in detecting Cr₂O₇²⁻ and CrO₄²⁻ ions, the corresponding fluorescence evolution experiments were then carried out by gradually increase the concentrations from 0 to 390 μM for Cr₂O₇²⁻ and 0–675 μM for CrO₄²⁻, respectively. And the changes of their fluorescence emission intensities at the maximum emission wavelength were monitored synchronously by fluorescence spectrophotometer. As illustrated in Fig. 7a, the fluorescence emission peak of **1** at 373 nm attenuated gradually and finally almost transformed into a straight line, with the emission intensity decreased from 935.84 to 19.12 and quenching efficiency of 97.96%. For CrO₄²⁻ ions, the similar fluorescence evolution details also were recorded as shown in Fig. S14a, with a calculated quenching efficiency of 99.76%. In addition, the direct experimental evidences visible to the naked eyes are monitored as exhibited in Fig. S10. Moreover, based on the analysis of fluorescence evolution data, the detection limit values for Cr₂O₇²⁻ and CrO₄²⁻ are determined to be 4.83 and 2.84 ppb, respectively, both of which are fairly low results for reported MOFs based fluorescence sensing probes (Table S3). Besides, as revealed in Fig. 7b and Fig. S14b, when increasing the concentrations of Cr₂O₇²⁻ and CrO₄²⁻ ions, the I₀/I for **1** both raised rapidly, performing the high K_{sv} values of 2.45 × 10⁴ and 1.1 × 10⁴ M⁻¹, respectively, indicating that Cd-MOF of **1** is a very sensitive photochemical sensors.

More interestingly, as shown in Fig. 7c and Fig. S14c, when plotting the concentrations of Cr₂O₇²⁻ or CrO₄²⁻ ions in the aqueous suspension with fluorescence quenching efficiencies, we find that the curves can match perfectly with the Langmuir model, with corresponding correction coefficients of 0.999 and 0.998. Notably, this nearly perfect matching linear relationship in the whole detection concentration range indicates that compound **1** can quantitatively detect both Cr₂O₇²⁻ and CrO₄²⁻ analytes in a fairly wide concentration range, and is a very promising fluorescent probe material.

2.5. Mechanisms for fluorescence quenching sensing

As shown in Fig. 8, the PXRD diffraction peak intensity of compound **1** is still very strong after soaking in Pb²⁺, Cr₂O₇²⁻ and CrO₄²⁻ ions aqueous solution. Also, their diffraction peak position is very consistent with that of the as synthesized **1**. As a result, the fluorescence quenching sensing caused by the collapse of the Cd-MOF skeleton in aqueous solution due to the hydrolysis of the coordination bonds should firstly be eliminated [49].

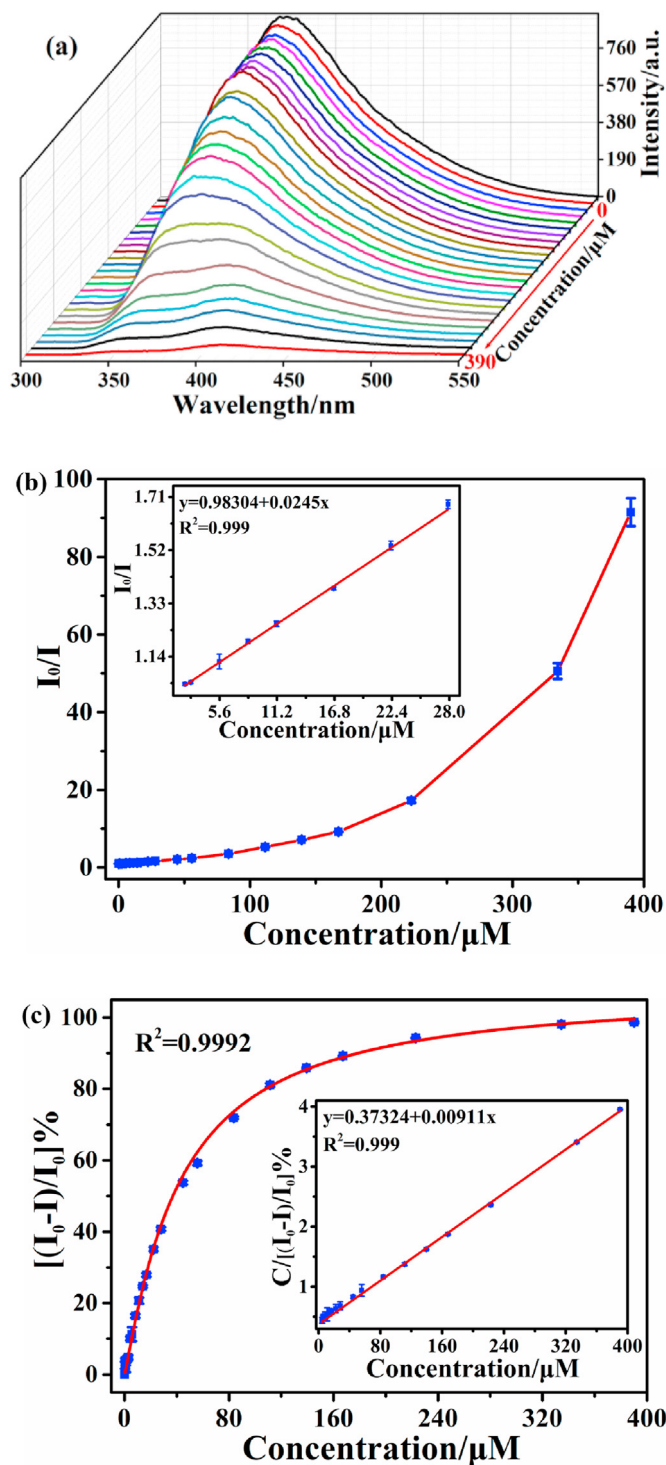


Fig. 7. Fluorescence sensing of **1** towards Cr₂O₇²⁻: (a) Concentration-dependent luminescence quenching of **1** towards Cr₂O₇²⁻. (b) Stern-Volmer plot of I_0/I versus Cr₂O₇²⁻ (inset: enlarged view of a selected area). (c) Simulated correlation between quenching ratio $(I_0 - I)/I_0$ and Cr₂O₇²⁻ concentration using the Langmuir model (inset: relationship between Cr₂O₇²⁻ concentration and $C/[(I_0 - I)/I_0]$).

2.5.1. Quenching mechanism towards Cr(VI) ions

In addition, by virtue of the comparison of UV-Vis absorption spectrum and fluorescence emission spectrum as shown in Fig. 9a and Fig. S15, we found that the wavelength range covered by one of the main UV-vis absorption bands of target analytes i. e. Cr₂O₇²⁻ and CrO₄²⁻ ions (220–312 nm) almost absolutely overlap with the fluorescence excitation wavelength range required by the aqueous suspension solution of **1**

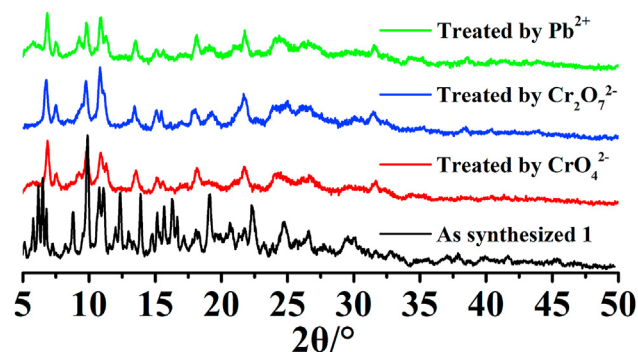


Fig. 8. The PXRD patterns of **1** after being treated by Pb(II) and Cr(VI) ions.

(220–330 nm). The largely overlap of absorption band and the excitation band between analytes and photochemical sensor indicates that the light energy used to excite Cd-MOF will be fully intercepted or consumed by Cr₂O₇²⁻ and CrO₄²⁻ ions, resulting in significant fluorescence quenching [46]. Moreover, the fluorescence emission band of Cd-MOF (330–513 nm) completely covers another major absorption bands of Cr₂O₇²⁻ (344–450 nm) and CrO₄²⁻ (338–432 nm) ions, indicating that the resonance energy of excited Cd-MOF is highly likely to transfer to Cr(VI) analytes surrounding the photochemical sensor and then cause fluorescence quenching [38]. Interestingly, as shown in Figs. S16 and S17, for other anions and cations, the weak overlapping performances of UV-vis absorption bands with excitation/emission wavelength ranges of **1** flawlessly match their bad fluorescence quenching induction abilities. From the opposite side, this also proves the rationality of the proposed Cr(VI)-induced fluorescence quenching mechanisms. Further, according to the almost unchanged X-ray photoelectron spectroscopy (XPS) curves of **1** before and after being immersed in Cr(VI) aqueous solution (Fig. 10), coordination reactions between **1** and Cr₂O₇²⁻/CrO₄²⁻ should be excluded. Therefore, the effective competitive capture of excited light energy and the strong acceptance of vibrational energy from excited states Cd-MOF by Cr(VI) ions should be the most important causes of fluorescence quenching.

2.5.2. Quenching mechanism towards Pb(II) ions

The fluorescence quenching of **1** caused by Pb²⁺ ions, however, is another case. As demonstrated in Fig. 9b, the UV-Vis absorption bands of Pb(NO₃)₂, fluorescence excitation and emission bands of Cd-MOF are independent of each other and almost do not overlap at all. The interception of excited light energy by Pb²⁺ ions and the transfer of resonance energy from Cd-MOF to analytes thus should be unrelated to fluorescence quenching. Generally, luminescent MOFs with abundant functional groups (free Lewis basic active sites) are more sensitive to analytes in water, because the free metal ions (Lewis acid) in aqueous solution tend to coordinate with these free sites, and then lead to the quenching response of MOFs based probes [50–52]. For Cd-MOF of **1**, considering that its framework comprises a large number of uncoordinated imidazole N atoms from —NH— groups and carboxyl O atoms in monodentate coordination fashion with Cd(II) centres (Fig. 1a), the free guest Pb(II) ions in aqueous solution are highly likely to interact with these free anchoring sites, thus causing fluorescence quenching of **1**. Here, this inference was carefully verified using XPS and FT-IR characterization techniques. As clearly revealed in Fig. 11a and b, compared with fresh **1**, striking Pb_{4f} peak was monitored on Cd-MOF after being immersed in Pb(II) aqueous solution, confirming the generation of new bonds between Pb(II) analytes and the framework. In addition, high-resolution XPS spectra of N1s region for **1** before and after incorporated with Pb(II) ions also was studied. Here, the N1s region of fresh **1** was dissected into three peaks with binding energy of 399.90, 398.85 and 400.48 eV (Fig. 11c), which should be respectively assigned to the uncoordinated N atoms of C=NH and C–N bonds in benzimidazole rings. While obvious

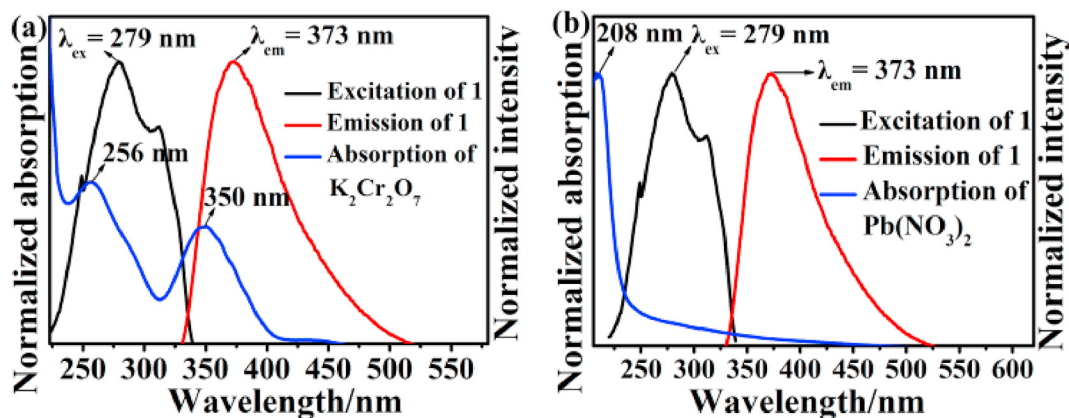


Fig. 9. UV-vis absorption spectra of $\text{Cr}_2\text{O}_7^{2-}$ (a) and Pb^{2+} (b) ions, as well as the excitation and emission spectrum of **1**.

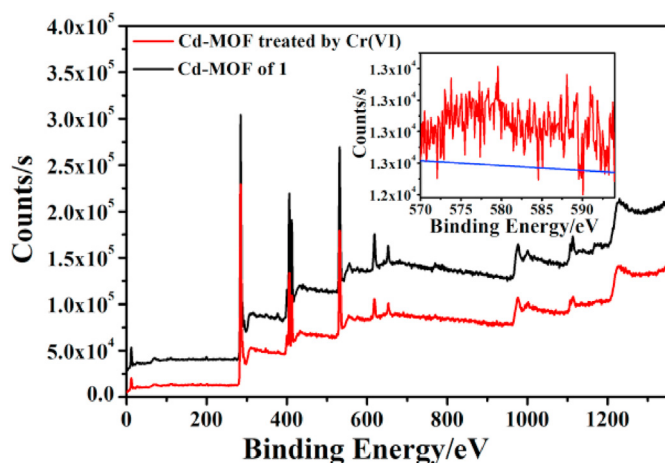


Fig. 10. XPS spectrum of **1** before and after treated by Cr(VI), the inset shows high-resolution XPS spectrum of Cr 2p region from Cr(VI) treated **1**.

shift for three peaks was observed at 398.78, 397.93 and 399.94 eV (Fig. 11d), indicating the coordination between Pb(II) ions and N atoms [38,53]. Moreover, the coordination of Pb(II) ions with carboxyl O atom has also been confirmed, according to the newly generated $\text{O}1s$ peak at 530.9 eV (Fig. 11e and f) from XPS spectra and the completely disappeared stretching vibration peaks of carboxyl groups at 1655 cm^{-1} from FT-IR spectra of $\text{Pb}(\text{NO}_3)_2$ aqueous solution treated **1** (Fig. S18) [45, 54]. In conclusion, both the shift of $\text{N}1s$ and $\text{O}1s$ peaks confirmed by XPS measurement and the disappearance of $-\text{COO}-$ groups determined by FT-IR characterization suggest that the coordination reactions between Pb(II) analytes and Cd-MOF occurred, which lead to the fluorescence quenching response of **1**.

2.6. Photocatalytic reduction removal of Cr(VI)

Given that the typical semiconductor characteristics of cadmium oxide and the excellent photosensitivity of highly conjugated aromatic ligands H_3L (Fig. 2 and Fig. S4), Cd-MOF of **1** which assembled from the four connected Cd-O/Cd-N metal nodes and deprotonated H_3L linkers is entirely likely to be an effective photocatalyst for reducing Cr(VI) to usually considered Cr(III) [55]. Firstly, as shown in Fig. S19, according to the recorded UV-Vis diffuse-reflectance spectrum (DRS), compound **1** exhibit a broader UV-Vis absorption bands from 200 to 450 nm. And its energy band gaps (Eg) value was calculated to be 3.3 eV by virtue of the widely used Kubelka-Munk equation and this value just locate in the semiconductor region. Since the UV-Vis absorption wavelength coverage of compound **1** is mainly located in the UV region, the mercury lamp of

500 W was employed to conduct photocatalytic reduction studies of Cr(VI). Before starting the photocatalytic reduction process, solid samples of **1** were immersed in $\text{K}_2\text{Cr}_2\text{O}_7$ aqueous solution overnight to obtain adsorption-desorption equilibrium in the dark. As depicted in Fig. 12a, with the extension of irradiation time, the absorption band intensity of $\text{Cr}_2\text{O}_7^{2-}$ at 350 nm decreased rapidly and disappeared almost completely just within 40 min. At the same time, the color of $\text{K}_2\text{Cr}_2\text{O}_7$ aqueous solution visible to the naked eyes also faded to colorless. Then, by virtue of the absorbance-concentration calibration curve (Fig. S20), the concentration of residual $\text{Cr}_2\text{O}_7^{2-}$ ions in the photocatalytic reduction product was quantified to be 0 mg L^{-1} at 40 min from original 28.9 mg L^{-1} , with the photochemical reduction efficiency of 100% (Fig. 12b). Correspondingly, the reduction rate constant was determined to be as high as 0.071 min^{-1} (Fig. 12c) according to apparent first-order rate equation, indicating the fairly high efficiency of **1** in photochemical elimination towards $\text{Cr}_2\text{O}_7^{2-}$ (Table S4).

In addition, photochemical stability and hydrolysis resistance stability are essential for a practical photocatalyst. Therefore, the catalytic recyclability for Cd-MOF of **1** was deliberately confirmed by carrying out consecutive seven photochemical reduction cycles towards potassium dichromate aqueous solution of 28.9 mg L^{-1} , under the irradiation of 500 W mercury lamp within 40 min. As exhibited in Fig. 12d, well-preserved photocatalytic reduction performance was confirmed throughout the whole recycling experiment. Interestingly, compared with the catalytic efficiency of over 100% at first, a fairly high value of still up to 92.0% was recorded at the 7th cycle, revealing the excellent recyclability of **1** for practical application.

It is really essential to clarify the photocatalytic reduction products of $\text{Cr}_2\text{O}_7^{2-}$ ions catalyzed by Cd-MOF of **1**. Researchers generally believe that Cr^{3+} ions should be the final photocatalytic reduction product [19, 20]. Here, a control experiment thus was designed to confirm this hypothesis. Fresh $\text{Cr}(\text{NO}_3)_3$ aqueous solution was deliberately prepared as a blank control to compare with the photocatalytic reduction products of compounds **1**. Firstly, as revealed in Fig. S21, the UV-Vis absorption curves of photocatalytic reduction products supernatant and fresh $\text{Cr}(\text{NO}_3)_3$ aqueous solution matched well with each other, indicating that the photocatalytic reduction product of $\text{Cr}_2\text{O}_7^{2-}$ should be Cr^{3+} ion. Secondly, from the visual experiment, when excessive NaOH were added into above two aqueous solutions, dark green floccule were formed in both scintillation vials (Fig. S22) containing photochemical reduction products supernatant and $\text{Cr}(\text{NO}_3)_3$ aqueous solution, respectively. Therefore, combine the above research results, the final products of $\text{Cr}_2\text{O}_7^{2-}$ reduced by Cd-MOF of **1** under lighted mercury lamp was determined to be less toxic Cr^{3+} ions. The reaction equation should be as follows: $\text{Cr}(\text{NO}_3)_3 + 3\text{NaOH} = \text{Cr}(\text{OH})_3 + 3\text{NaNO}_3$.

Considering that the possibility of coordination of Cr(VI) ions with Cd-MOF has been excluded (Fig. 10), we speculate that $\text{Cr}_2\text{O}_7^{2-}$ ions obtain the necessary electrons for its reduction by contact/collision with

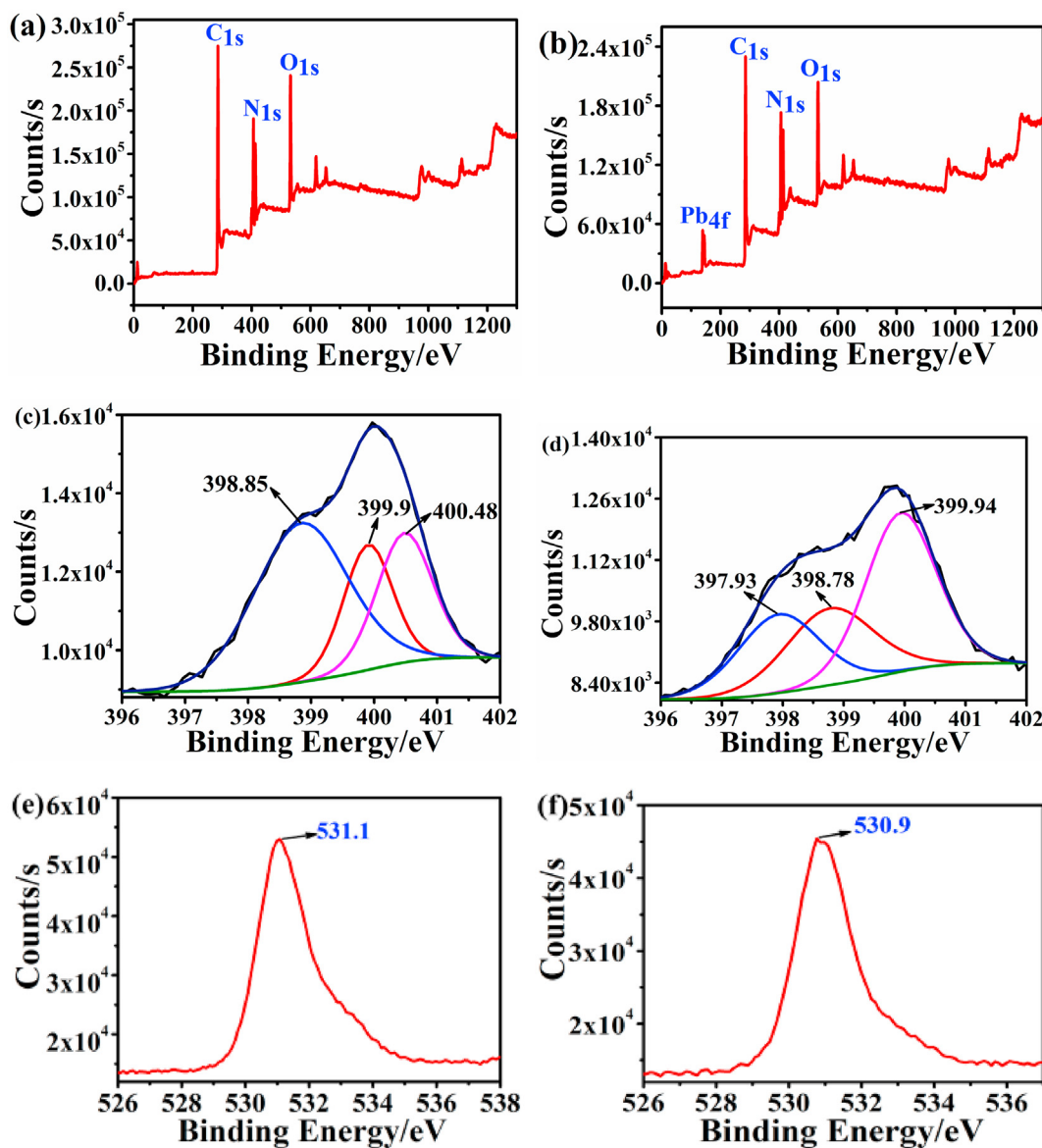


Fig. 11. XPS spectrum of as synthesized **1**(a) and Pb(II) incorporated **1**(b), high-resolution XPS spectrum for N_{1s} region of **1**(c) and Pb(II) incorporated **1**(d), high-resolution XPS spectrum for O_{1s} region of **1**(e) and Pb(II) incorporated **1**(f).

the framework of photoexcited compound **1**. That is, the highly conjugated three-connected matrix **L** play the role of optical absorption antenna which can achieve optical energy from UV illuminant and transfer the photogenerated electrons to catalytic center quickly, leaving the positively charged holes (h^+) on valence band (VB) [27,56]. Then, the reductive electrons excited to conduction band (CB) will be captured by highest valence state $\text{Cr}_2\text{O}_7^{2-}$ ions and then reduced them to Cr^{3+} at lower valence states. To further clarify the electronic structure of **1** and find out its photocatalytic removal details in reducing Cr(VI), the electrochemical properties for solid powder of **1** were verified by Mott-Schottky technique. As shown in Fig. 13, three Mott-Schottky curves of **1** were obtained at 6000, 6500 and 7000 Hz, respectively. And their positive tangent slopes strongly suggest the n typed semiconductor characteristics of Cd-MOF [57]. According to Mott-Schottky and Nernst equation, the flat band potential (V_{fb}) of semiconductors was estimated from the x intercept of curve fitting and could be assumed to be the position of conduction band (CB). Here, the potential value of CB on **1** was determined to be -2.72 eV, fairly low a potential value, according to the intercept value of tangent intersection for three curves on the x axis. Then, the valence band (VB) potential value of **1** can be calculated to be

0.58 eV by adding the CB value to the E_g value (3.3 eV). Ingeniously, as exhibited in Fig. 14, the potential value of CB is much more negative than the potential of $+1.35$ eV for $\text{Cr}_2\text{O}_7^{2-}/\text{Cr}^{3+}$ [58,59], indicating that the electronic structure of **1** is suitable to drive efficient and rapid photocatalytic reduction reaction and further reduce the highly toxic Cr(VI) to friendly Cr(III). And this logic perfectly matched the excellent performances of **1** in photocatalytic reduction experiments. The corresponding reaction process should be as follows: $\text{Cr}_2\text{O}_7^{2-} + 14\text{H}^+ + 6\text{e}^- \rightarrow 2\text{Cr}^{3+} + 7\text{H}_2\text{O}$

3. Conclusions

In summary, a novel Cd(II)-MOF of **1** has been assembled using an asymmetric triangular shaped carboxylate ligand. Compound **1** presents a 2D plane comprising of two parallel but closely connected single networks, and further stack into the final 3D framework decorated with rich imidazole N atoms and carboxyl O atoms. Prominently, **1** performed effective/persistent photoluminescence capability, instantaneous fluorescence quenching response detection towards Pb^{2+} , $\text{Cr}_2\text{O}_7^{2-}$ and CrO_4^{2-} ions with ultra low detection limits (DL) of 1.89, 4.83 and 2.84 ppb, fairly

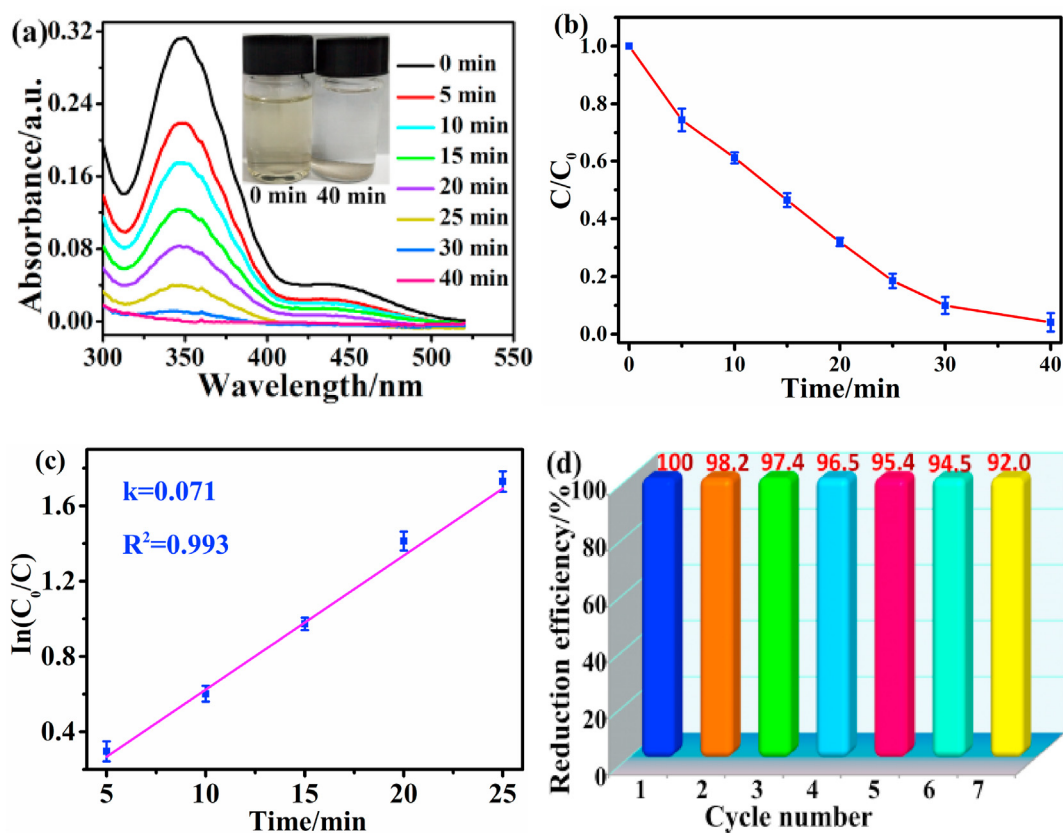


Fig. 12. Changes of UV-Vis spectra with time (a), corresponding plots of C/C_0 versus time (b), pseudo first order kinetic curve (c), photocatalytic reduction efficiency changes in 7 consecutive cycles (d).

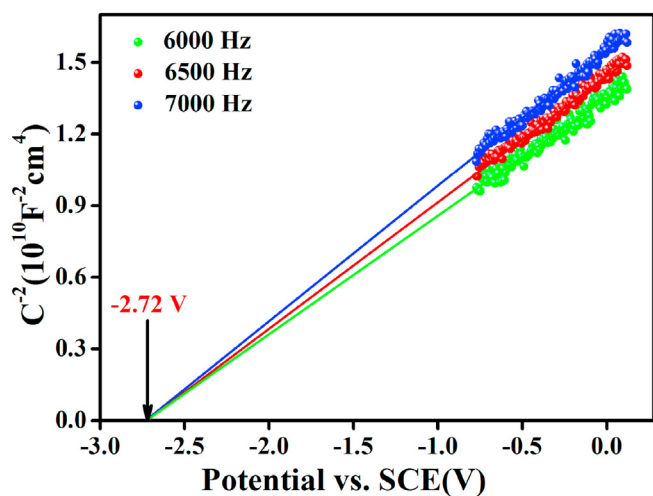


Fig. 13. Mott-Schottky plots of 1.

high K_{sv} values of 2.40×10^4 , 2.45×10^4 and $1.1 \times 10^4 \text{ M}^{-1}$, respectively. Prominently, Cr(VI) can be reduced to Cr(III) by 1 under the irradiation of UV light just within 40 min, with fairly high photocatalytic reduction efficiency of 100%, reduction rate constant of 0.071 min^{-1} and reliable recycling capacity of more than 7 times. This work provides a highly efficient and bifunctional Cd(II)-MOF platform for Pb(II), Cr(VI) detection and Cr(VI) photoreduction, and may open a new avenue for addressing the fatal environmental pollution issues caused by heavy metal ions.

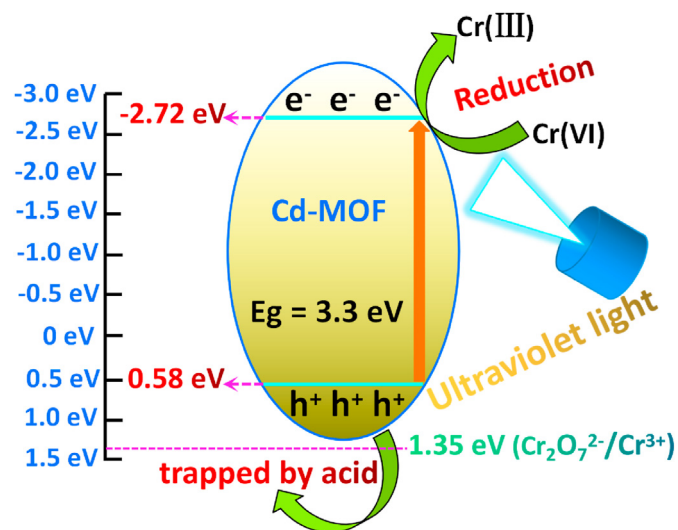


Fig. 14. Schematic of proposed photocatalytic reduction mechanism of 1 towards Cr(VI).

4. Experimental

4.1. Materials and instrumentation

The organic ligand of H_3L , $\text{Cd}(\text{NO}_3)_2$, N, N-dimethylformamide and all chemical reagents were obtained by commercial suppliers and used without further purification. The powder X-ray diffraction (PXRD) data were collected over a MiniFlex600 X-ray diffractometer with $\text{Cu K}\alpha$ ($\lambda = 1.54$

= 1.5406 Å). The X-ray tube was operated at 40 kV (40 mA), with the diffraction angle range of 5–55° and scanning rate of 10° min⁻¹. Fourier-transform infrared (FT-IR) spectrum was collected in the solid state of KBr pellet over a Nicolet 5700 FT-IR spectrometer with a wave number range from 4000 to 400 cm⁻¹. The Fluorescence excitation or emission spectra of the **1** were measured on a Shimadzu RF5301 fluorescence spectrophotometer at room temperature. UV–vis spectra for targets were carried out on a Shimadzu UV2450 UV–vis spectrophotometer. UV–Vis diffuse reflection spectra were performed on a HITACHI U3310 spectrophotometer with BaSO₄ as the background. Thermogravimetric curve was recorded on a METTLER TOLEDO TGA/SDTA851e analyzer which was carried out under N₂ atmosphere with heating rate of 10 °C/min under the temperature range of 25–800 °C. The binding energy of **1** were analyzed by X-ray photoelectron spectroscopy (XPS) from Thermo Escalab 250Xi with a monochromatic Al Kα (hν = 1486.6 eV). The measurements for the Mott-Schottky plots were performed on an electrochemical workstation (Bio Logic VSP-300, Germany) in a standard three-electrode system configuration using probe solution as the electrolyte at the frequencies of 6000, 6500 and 7000 Hz, respectively.

4.2. Synthesis of Cd-MOF of **1**

Cd(NO₃)₂ (0.01 mol, 3.1 mg), H₃L (0.01 mol, 4.8 mg) were dissolved in the solvent of DMF/H₂O (volume ratio = 3/2) and transferred into a 20 mL scintillation vial. After ultrasonic dispersion for 20 min, the mixture was heated at 85 °C for 24 h and then increased to 115 °C for 72 h. After naturally cooling to room temperature, colourless block-shape crystals of **1** were collected and washed by fresh DMF for 3 times.

4.3. Fluorescence evolution, selective and anti-interference experiments

For fluorescence evolution experiments, lead nitrate, potassium dichromate and potassium chromate were used as the sources of lead (Pb²⁺) and Cr(VI) (Cr₂O₇²⁻, CrO₄²⁻), respectively. Here, 10 mg fresh sample of **1** was ground and dispersed into deionized water, and further being ultrasonically dispersed for 10 min to form the monodisperse suspension of **1** with solid-liquid ratio of 16 mg L⁻¹. Then a series of uniformly mixed aqueous suspensions of Pb²⁺/1, Cr₂O₇²⁻/1 and CrO₄²⁻/1 were formed by adding 50 μL Pb²⁺, Cr₂O₇²⁻ or CrO₄²⁻ solution (concentration from 0.099 to 30 μM, 0.27863–390 μM and 0.422–675 μM) into a quartz cuvette which containing 3 mL above aqueous suspension of **1**. Immediately, the quenching properties of Cr₂O₇²⁻/1, CrO₄²⁻/1 and Pb²⁺/1 were monitored by fluorescence spectrophotometer with the excitation wavelength of 279 nm and the emission wavelength of 220–600 nm.

In the selective and anti-interference experiments, 50 μL aqueous solutions of metal cations from nitrates (Na⁺, Cd²⁺, Cr³⁺, Mg²⁺, K⁺, Cu²⁺, Fe³⁺, Ag⁺, Co²⁺ and Ni²⁺), anionic aqueous solutions from potassium salts (I⁻, F⁻, IO₃⁻, NO₂⁻, Cl⁻, Br⁻, SO₄²⁻, SCN⁻, C₂H₅O⁻, PO₄³⁻, CO₃²⁻ and HPO₄²⁻), as well as aqueous solutions of Pb²⁺, Cr₂O₇²⁻ and CrO₄²⁻ were prepared and then added into 3 mL of the above aqueous suspensions of **1**, respectively. The concentrations of final aqueous suspension for Pb²⁺, single and mixed anions/cations were set to be 30 μM. For Cr₂O₇²⁻, single and mixed anions/cations, the final concentrations of aqueous suspension were determined to be 3.9 × 10² μM. As for CrO₄²⁻ research system, the values of single and mixed concentrations were set to be 6.75 × 10² μM. Herein, the blank control sample was prepared by introducing 50 μL deionized water into 3 mL above-mentioned aqueous suspension of **1**. The fluorescence intensity of each sample was recorded by fluorescence spectrophotometer.

4.4. Photocatalytic reduction towards Cr(VI)

Photocatalytic reduction studies of **1** towards Cr(VI) were carried out by adding 30 mL Cr(VI) aqueous solution of 30 mg L⁻¹ into a 30 mL quartz tube containing 10 mg as synthesized **1**. The pH values of reaction system were adjusted by diluted HCl or NaOH aqueous solution, and

formic acid was adopted as hole trapping agent. Before turning on the 500 W mercury lamp, the saturated adsorption-desorption process was carried out by soaking **1** in Cr(VI) aqueous solution for more than 12 h. After replacing Cr(VI) aqueous solution with fresh one (30 mg L⁻¹), the quartz reaction tubes would be transferred into the photochemical reactor. Continuous air flow would be pumped into the bottom of reactors to maintain solid samples of **1** suspended in aqueous solution. Then, the photocatalytic reduction reaction began under the irradiation of ultraviolet light. Changes of absorbance values for Cr(VI) ions at the maximum absorption wavelength (350 nm) were monitored by a UV–Vis spectrophotometer. Moreover, the recorded absorbance values at different time intervals were utilized to calculate the photochemical reduction ratio using the following equation:

CRedit authorship contribution statement

Ling-Hui Chen: Methodology, Investigation, Writing – original draft. **Xin-Bin Cai:** Writing – original draft, Supervision. **Qing Li:** Conceptualization, Methodology, Writing – review & editing. **Bin-Bin Guan:** Investigation, Supervision. **Tian-Hui Liu:** Investigation, Supervision. **Dan Li:** Synthesis of MOFs, Characterization. **Zhi-Qiang Wu:** Synthesis of MOFs, Characterization. **Wei Zhu:** Validation, Conceptualization, Formal analysis.

Declaration of competing interest

The authors declare that they have no known competing financial interests or personal relationships that could have appeared to influence the work reported in this paper.

Acknowledgments

We acknowledge the financial support of the National Natural Science Foundation of China (No. 22078253), the Xi'an Science and Technology Project of China (No. 2019217114GXRC007CG008-GXYD7.1), the Graduate Scientific Innovation Fund for Xi'an Polytechnic University (No. chx2021021), the Shaanxi Provincial Education Department Service Local Special Project (No. 19JC016) and Science and Technology Project of Beilin District in Xi'an (No. GX2003).

Appendix A. Supplementary data

Supplementary data to this article can be found online at <https://doi.org/10.1016/j.jssc.2021.122416>.

References

- [1] R.R. Pawar, H.C. Bajaj Lalhmunsiana, S.-M. Lee, *J Ind Eng Chem* 34 (2016) 213–223.
- [2] H. Lalhruaitluanga, K. Jayaram, M.N. Prasad, K.K. Kumar, *J. Hazard. Mater.* 175 (2010) 311–318.
- [3] M. Feng, P. Zhang, H.-C. Zhou, V.K. Sharma, *Chemosphere* 209 (2018) 783–800.
- [4] P.A. Kobielska, A.J. Howarth, O.K. Farha, S. Nayak, *Coord Chem Rev* 358 (2018) 92–107.
- [5] S. Couck, J.F.M. Denayer, G.V. Baron, T. Rémy, J. Gascon, F. Kapteijn, *J. Am. Chem. Soc.* 131 (2009) 6326–6327.
- [6] S. Sanchez, R. Perez Aguilar, S. Genta, M. Aybar, E. Villecco, A. Sanchez Riera, *J Appl Toxicol* 21 (2001) 417–423.
- [7] J. Sun, P. Guo, M. Liu, H. Li, *J. Mater. Chem. C* 7 (2019) 8992–8999.
- [8] A.V. Desai, B. Manna, A. Karmakar, A. Sahu, S.K. Ghosh, *Angew. Chem. Int. Ed.* 55 (2016) 7811–7815.
- [9] T.-J. Jiang, M. Yang, S.-S. Li, M.-J. Ma, N.-J. Zhao, Z. Guo, J.-H. Liu, X.-J. Huang, *Anal. Chem.* 89 (2017) 5557–5564.
- [10] M. Lu, Y. Deng, Y. Luo, J. Lv, T. Li, J. Xu, S.-W. Chen, *J. Wang, Anal. Chem.* 91 (2019) 888–895.
- [11] H.N. Rubin, M.M. Reynolds, *Inorg. Chem.* 58 (2019) 10671–10679.
- [12] Z.-Q. Yao, G.-Y. Li, J. Xu, T.-L. Hu, X.-H. Bu, *Chem. Eur. J.* 24 (2018) 3192–3198.
- [13] S. Bahrami, M.R. Yafian, P. Najvak, L. Dolatyari, H. Shayani-Jam, S.D. Kolev, *Sep. Purif. Technol.* 250 (2020) 117251.
- [14] M. He, L. Wang, Z. Zhang, Y. Zhang, J. Zhu, X. Wang, Y. Lv, R. Miao, *ACS Appl. Mater. Interfaces* 12 (2020) 57102–57116.

- [15] X. Huang, D. Wei, X. Zhang, D. Fan, X. Sun, B. Du, Q. Wei, *Sci. Total Environ.* 685 (2019) 681–689.
- [16] S. Li, F. Yang, J. Li, K. Cheng, *Sci. Total Environ.* 746 (2020) 141037.
- [17] E.C. Nnadozie, P.A. Ajibade, *Microporous Mesoporous Mater* 309 (2020) 110573.
- [18] Q. Yu, J. Guo, Y. Muhammad, Q. Li, Z. Lu, J. Yun, Y. Liang, *J. Environ. Manage.* 276 (2020) 111245.
- [19] H. Kaur, S. Sinha, V. Krishnan, R.R. Koner, *Ind. Eng. Chem. Res.* 59 (2020) 8538–8550.
- [20] D.-M. Chen, C.-X. Sun, C.-S. Liu, M. Du, *Inorg. Chem.* 57 (2018) 7975–7981.
- [21] S. Yuan, J.-S. Qin, L. Zou, Y.-P. Chen, X. Wang, Q. Zhang, H.-C. Zhou, *J. Am. Chem. Soc.* 138 (2016) 6636–6642.
- [22] C. Fan, B. Zhu, X. Zhang, C. Bi, D. Zhang, Z. Zong, Y. Fan, *Inorg. Chem.* 60 (2021) 6339–6348.
- [23] C. Fan, X. Zhang, N. Li, C. Xu, R. Wu, B. Zhu, G. Zhang, S. Bi, Y. Fan, *J. Pharm. Biomed. Anal.* 188 (2020) 113444.
- [24] C. Fan, C. Xu, B. Zhu, L. Wang, Z. Zong, R. Wu, X. Zhang, Y. Fan, *J. Solid State Chem* 298 (2021) 122157.
- [25] Y. Yan, C.Q. Li, Y.H. Wu, J.K. Gao, Q.C. Zhang, *J. Mater. Chem. A* 8 (2020) 15245–15270.
- [26] C. Li, K.B. Wang, J.Z. Li, Q.C. Zhang, *ACS Materials Lett* 2 (7) (2020) 779–797.
- [27] Y.Y. Sun, D.F. Lu, Y.X. Sun, M.Y. Gao, N. Zheng, C. Gu, F. Wang, J. Zhang, *ACS Materials Lett* 3 (2021) 64–68.
- [28] K. Wang, Q. Li, Z. Ren, C. Li, Y. Chu, Z. Wang, M. Zhang, H. Wu, Q. Zhang, *Small* 16 (2020) 2001987.
- [29] K.-B. Wang, Q. Xun, Q. Zhang, *EnergyChem* 2 (2020) 100025.
- [30] K. Wang, Z. Wang, J. Liu, C. Li, F. Mao, H. Wu, Q. Zhang, *ACS Appl. Mater. Interfaces* 12 (2020) 47482–47489.
- [31] K. Wang, S. Wang, J. Liu, Y. Guo, F. Mao, H. Wu, Q. Zhang, *ACS Appl. Mater. Interfaces* 13 (2021) 15315–15323.
- [32] T. Rasheed, F. Nabeel, *Coord Chem Rev* 401 (2019) 213065.
- [33] Z. Hu, B.J. Deibert, J. Li, *Chem. Soc. Rev.* 43 (2014) 5815–5840.
- [34] H.R. Fu, X.X. Wu, L.F. Ma, F. Wang, J. Zhang, *ACS Appl. Mater. Interfaces* 10 (2018) 18012–18020.
- [35] Y. Zhao, Y.-J. Wang, N. Wang, P. Zheng, H.-R. Fu, M.-L. Han, L.-F. Ma, L.-Y. Wang, *Inorg. Chem.* 58 (2019) 12700–12706.
- [36] H. Yu, M. Fan, Q. Liu, Z. Su, X. Li, Q. Pan, X. Hu, *Inorg. Chem.* 59 (2020) 2005–2010.
- [37] S. Jindal, V.K. Maka, J.N. Moorthy, *J. Mater. Chem. C* 8 (2020) 11449–11456.
- [38] Q. Li, B.-B. Guan, W. Zhu, T.-H. Liu, L.-H. Chen, Y. Wang, D.-X. Xue, *J. Solid State Chem* 291 (2020) 121672.
- [39] B.-B. Guan, Q. Li, Y.-T. Xu, L.-H. Chen, Z. Wu, Z.-L. Fan, W. Zhu, *Inorg Chem Commun* 122 (2020) 108273.
- [40] C. Xu, Y. Pan, G. Wan, H. Liu, L. Wang, H. Zhou, S.-H. Yu, H.-L. Jiang, *J. Am. Chem. Soc.* 141 (2019) 19110–19117.
- [41] W.-M. Liao, J.-H. Zhang, Z. Wang, Y.-L. Lu, S.-Y. Yin, H.-P. Wang, Y.-N. Fan, M. Pan, C.-Y. Su, *Inorg. Chem.* 57 (2018) 11436–11442.
- [42] Q. Li, X. Cai, L.-H. Chen, B.-B. Guan, Z.-L. Fan, W. Zhu, D.-X. Xue, *Inorg. Chem.* 60 (2021) 8143–8153.
- [43] R.-X. Yao, X. Cui, X.-X. Jia, F.-Q. Zhang, X.-M. Zhang, *Inorg. Chem.* 55 (2016) 9270–9275.
- [44] G. Ji, J. Liu, X. Gao, W. Sun, J. Wang, S. Zhao, Z. Liu, *J. Mater. Chem. A* 5 (2017) 10200–10205.
- [45] J.-J. Huang, J.-H. Yu, F.-Q. Bai, J.-Q. Xu, *Cryst. Growth Des.* 18 (2018) 5353–5364.
- [46] R. Lv, H. Li, J. Su, X. Fu, B. Yang, W. Gu, X. Liu, *Inorg. Chem.* 56 (2017) 12348–12356.
- [47] A. Karmakar, A.V. Desai, S.K. Ghosh, *Coord Chem Rev* 307 (2016) 313–341.
- [48] G. He, H. Peng, T. Liu, M. Yang, Y. Zhang, Y. Fang, *J. Mater. Chem.* 19 (2009) 7347–7353.
- [49] M. Singh, S. Senthilkumar, S. Rajput, S. Neogi, *Inorg. Chem.* 59 (2020) 3012–3025.
- [50] Z. Hao, X. Song, M. Zhu, X. Meng, S. Zhao, S. Su, W. Yang, S. Song, H. Zhang, *J. Mater. Chem. A* 1 (2013) 11043–11050.
- [51] Y. Xiao, Y. Cui, Q. Zheng, S. Xiang, G. Qian, B. Chen, *ChemComm* 46 (2010) 5503–5505.
- [52] J.-Q. Liu, G.-P. Li, W.-C. Liu, Q.-L. Li, B.-H. Li, R.W. Gable, L. Hou, S.R. Batten, *ChemPlusChem* 81 (2016) 1299–1304.
- [53] X. Luo, L. Ding, J. Luo, *J. Chem. Eng. Data* 60 (2015) 1732–1743.
- [54] S.-W. Lv, J.-M. Liu, C.-Y. Li, N. Zhao, Z.-H. Wang, S. Wang, *Chem. Eng. J.* 375 (2019) 122111.
- [55] C.-K. Lin, D. Zhao, W.-Y. Gao, Z. Yang, J. Ye, T. Xu, Q. Ge, S. Ma, D.-J. Liu, *Inorg. Chem.* 51 (2012) 9039–9044.
- [56] X.-D. Du, X.-H. Yi, P. Wang, W. Zheng, J. Deng, C.-C. Wang, *Chem. Eng. J.* 356 (2019) 393–399.
- [57] A.M. Huerta-Flores, L.M. Torres-Martínez, E. Moctezuma, A.P. Singh, B. Wickman, *J. Mater. Sci. Mater. Electron.* 29 (2018) 11613–11626.
- [58] R. Liang, L. Shen, F. Jing, W. Wu, N. Qin, R. Lin, L. Wu, *Appl. Catal. B* 162 (2015) 245–251.
- [59] X.Q. Qiao, Z.W. Zhang, Q.H. Li, D.F. Hou, Q.C. Zhang, J. Zhang, D.S. Li, P.Y. Feng, X.H. Bu, *J. Mater. Chem. A* 6 (2018) 22580–22589.